Relationship between compressive properties of human os calcis cancellous bone and microarchitecture assessed from 2D and 3D synchrotron microtomography.

Hélène Follet, Karine Bruyère-Garnier, Françoise Peyrin, Jean-Paul Roux, Monique E. Arlot, Brigitte Burt-Pichat, C. Rumelhart, Pierre J. Meunier

ELSEVIER

Bone 36 (2005) 340–351

BONE

www.elsevier.com/locate/bone

Relationship between compressive properties of human os calcis cancellous bone and microarchitecture assessed from 2D and 3D synchrotron microtomography

H. Follet[a], K. Bruyère-Garnier[a], F. Peyrin[b,c,*], J.P. Roux[d], M.E. Arlot[d], B. Burt-Pichat[d], C. Rumelhart[a], P.J. Meunier[d]

[a]*Laboratoire de Mécanique des Contacts et des Solides (LaMCoS) UMR CNRS 5514, INSA, Bât Coulomb, Lyon, France*
[b]*CREATIS, UMR CNRS 5515, Bât. Blaise Pascal, INSA, Lyon, France*
[c]*ESRF, BP 220, 38043 Grenoble Cedex, France*
[d]*Laboratoire d'Histodynamique Osseuse INSERM U403, Faculte Laennec, Lyon, France*

Received 23 July 2004; revised 29 September 2004; accepted 19 October 2004

Abstract

The aim of this study was to determine the contribution of 2D and 3D microarchitectural characteristics in the assessment of the mechanical strength of os calcis cancellous bone. A sample of cancellous bone was removed in a medio-lateral direction from the posterior body of calcaneus, taken at autopsy in 17 subjects aged 61–91 years. The sample was first used for the assessment of morphological parameters from 2D morphometry and 3D synchrotron microtomography (μCT) (spatial resolution = 10 μm). The 2D morphometry was obtained from three slices extracted from the 3D μCT images. Very good concordance was shown between 3D μCT slices and the corresponding physical histologic slices. In 2D, the standard histomorphometric parameters, fractal dimension, mean intercept length, and connectivity were computed. In 3D, histomorphometric parameters were computed using both the 3D mean intercept length method and model-independent techniques. The 3D fractal dimension and the 3D connectivity, assessed by Euler density, were also evaluated. The cubic samples were subjected to elastic compressive tests in three orthogonal directions (X, Y, Z) close to the main natural trabecular network directions. A test was performed until collapse of trabecular network in the main direction (Z). The mechanical properties were significantly correlated to most morphological parameters resulting from 2D and 3D analysis. In 2D, the correlation between the mechanical strength and bone volume/tissue volume was not significantly improved by adding structural parameters or connectivity parameter (nodes number/tissue volume). In 3D, one architectural parameter (the trabecular thickness, Tb.Th) permitted to improve the estimation of the compressive strength from the bone volume/tissue volume alone. However, this improvement was minor since the correlation with the BV/TV alone was high (r = 0.96). In conclusion, which is in agreement with the statistic's rules, we found, in this study, that the determination of the os calcis bone compressive strength using the 3D bone volume fraction cannot be improved by adding 3D architectural parameters.

Keywords: Bone morphometry; Computed tomography; Cancellous bone; Mechanical testing; Calcaneus

Introduction

It is widely accepted that aging leads to a loss of trabecular bone mass accompanied by modifications in trabecular microarchitecture [1–4]. Since the mechanical properties of a complex structure, such as the trabecular network, depend not only on the density but also on the micro-architecture and on the mechanical properties of its

* Corresponding author. ESRF, BP 220, 38043 Grenoble Cedex, France. Fax: +33 4 76 88 22 52.
E-mail addresses: hefollet@iupui.edu (H. Follet), karine.bruyere@inrets.fr (K. Bruyère-Garnier), peyrin@esrf.fr (F. Peyrin), Jean-Paul.Roux@sante.univ-lyon1.fr (J.P. Roux), Monique.Arlot@sante.univ-lyon1.fr (M.E. Arlot), Brigitte.Burt.pichat@sante.univ-lyon1.fr (B. Burt-Pichat), rumelhar@insa-lyon.fr (C. Rumelhart), Pierre.Meunier@sante.univ-lyon1.fr (P.J. Meunier).

8756-3282/$ - see front matter © 2004 Elsevier Inc. All rights reserved.
doi:10.1016/j.bone.2004.10.011

constitutive material, high failure risk for patients with osteoporosis appears clear [5,6]. In vivo, cancellous bone density is characterized by measurements of bone mineral density (BMD) using absorptiometric techniques, which do not see microarchitectural organization of bone. The relationships between density and mechanical properties of cancellous bone are well established but are not sufficient to estimate accurately the risk of fracture [7]. The additional role of trabecular micro-architecture in the mechanical properties has already been shown [8,9]. To quantify micro-architecture, histomorphometry is a reference 2D technique [1,10]. More recently, non-invasive techniques such as micro computed tomography (μCT) [11] or micro magnetic resonance imaging (μMRI) [12] have been proposed.

Histomorphometric parameters such as bone volume/tissue volume (BV/TV), trabecular thickness (Tb.Th), trabecular number (Tb.N), and trabecular separation (Tb.Sp) have been standardized [13] and are conventional descriptors of trabecular bone architecture. Others parameters have been proposed to quantify 2D anisotropy [10,14], 2D connectivity [15,16], and 2D irregularity [17,18]. Several studies already showed significant relationships between mechanical properties, histomorphometric parameters [19,20], and 2D fractal dimension [19]. Despite these significant relationships, it has not been proven that the best estimation of cancellous bone mechanical properties from density measurements is provided by adding 2D structural parameters. Furthermore, the limitation of 2D images to estimate the 3D architecture of trabecular networks has been shown in several works [21–25].

Different techniques are now available for computing standard or direct 3D parameters of bone samples from different anatomical human or animal sites [26,27]. Parameters quantifying 3D connectivity [24,28], 3D anisotropy [29], and 3D irregularity [17,30] can be extracted from 3D images. These methods have been used to characterize cancellous bone from different sites [31–34]. Even if 3D images may now be provided from different techniques and modalities, it is worthwhile noting that spatial resolution strongly affects the accuracy of architectural parameters [35,36]. 3D images of bone samples with a spatial resolution higher than 10 μm and high signal to noise ratio may easily be achieved using synchrotron radiation (SR) μCT [37,38].

The purpose of this work was to determine the respective contribution of conventional 2D structural and 3D architectural parameters in the estimation of compressive properties of human os calcis cancellous bone. 2D structural parameters were derived from morphometry, and 3D architectural parameters were extracted from very high-resolution 3D SR μCT. The statistical analysis should allow assessment of which parameters are likely to explain the variance of mechanical properties. Calcaneus cancellous bone has been chosen because, in vivo, this bone is an accessible site which easily allows DXA (Dual X-Ray Absorptiometry) and US (Ultrasound) measurements. Additionally, the calcaneus is used clinically as a good predictor of risk for hip and vertebrae fracture [16,39,40].

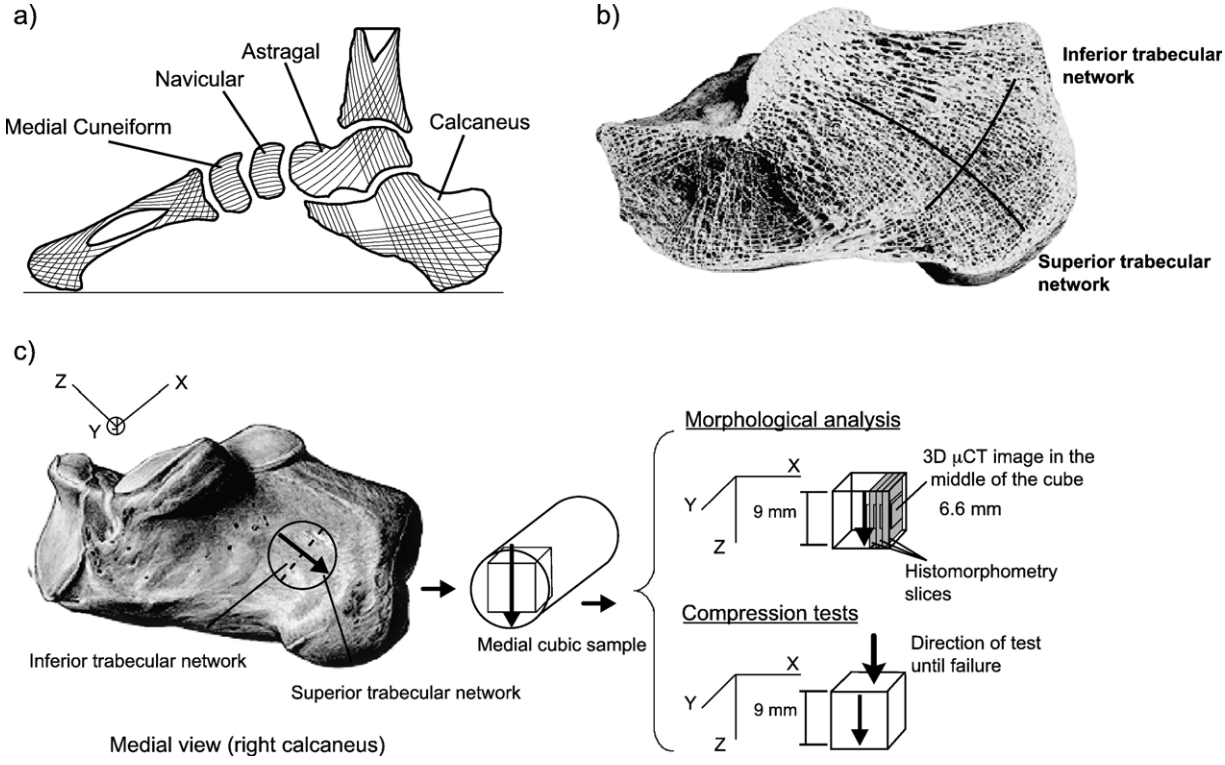

Fig. 1. Scheme of the trabecular structure in intern arch of foot by Kajandji [64] (a). Longitudinal cut and main trabecular network by Putz [65]. (b) Testing protocol showing the location of the cubic sample and the orientation for 3D imaging and (c) mechanical tests.

Material and methods

Material and protocol

Os calcis were excised at autopsy from 17 subjects (8 females, 9 males) aged [61–91] years (mean 78 ± 9 years).

Conventional radiographs (X-rays) were taken in the medio-lateral direction in order to exclude fractures and neoplastic lesions and to identify the superior network of the trabecular bone in the posterior body of the calcaneus (locate by an arrow in Fig. 1b) [41]. A cylindrical trabecular bone core (14.5 mm diameter) was drilled in the posterior body of the calcaneus along the medio-lateral axis (Y axis) (Fig. 1). Two contiguous cubic samples (9 mm/side, called "medial" and "lateral") oriented along the superior trabecular network (main trabecular direction, direction in which trabeculae are mainly oriented and called *Z* axis) were cut out of this core, using a low speed diamond water saw (Buehler, Iosmet®). In this study, only the medial cubic samples were used to perform all tests. The lateral cubic samples were embedded and one was used for the 2D morphometric analysis presented here; the remainder were used in other study. First, the frozen samples were imaged using 3D SR μCT imaging to obtain 3D and 2D morphometric parameters (Fig. 1c). Then, the same samples were dedicated to compressive tests. Between machining and mechanical testing, the samples were kept frozen, and before mechanical testing, they were placed in a 50% saline-ethanol solution for 3 days at 4°C for defrosting and at ambient temperature for 2–4 h [42].

3D synchrotron radiation μCT imaging

3D high-resolution tomographic images were acquired from SR μCT at the ESRF (Grenoble, France). SR μCT provides 3D images at very high spatial resolution with a high signal to noise ratio within a limited acquisition time [38]. Image acquisition was performed using a monochromatic X-ray beam fixed to 25 KeV. For each sample, 900 radiographic images (1024 × 1024), under different angles of view, were recorded. The spatial resolution in the recorded images was set to 10 μm, which has been previously shown to provide an accurate rendering of bone architecture while maintaining a significant field of view ($10 \times 10 \times 10$ mm^3) [36,43]. The 3D images were then obtained by applying an exact tomographic reconstruction algorithm, based on filtered-backprojection. The voxel size in the reconstructed images was $10 \times 10 \times 10$ μm. A centered 3D Region of Interest (ROI) made of $(660)^3$ voxels (6.6^3 mm^3) was selected in each sample for performance of the 3D architectural analysis.

3D morphometric analysis

The first step of image analysis was the segmentation of bone from background. Since the spatial resolution in the images was high (10 μm), partial volume effects were negligible. In addition, due to the high contrast and low noise level, the 3D images were easily segmented using simple thresholding. This assessment was confirmed by the observation of the histograms of the images, which clearly exhibited two classes, corresponding, respectively, to bone and to background. The same threshold, maximizing the interclass variance, was chosen for all samples.

After segmentation, 3D architectural parameters were computed from the 3D binary images. Parameters similar to those used in histomorphometry were computed using a 3D version of the mean intercept length (MIL) method [25,44]. For random directions in 3D space, the number of intercepts of a set of parallel test lines with the bone structure were computed and normalized by the total length of test lines. Then, the parameters were derived from the MIL based on the hypothesis of a parallel plate model [1]. The following parameters were used. Partial bone volume (BV/TV in %) represents the percentage of tissue occupied by bone. Parfitts' formulae [1,13] were used to calculate trabecular thickness (Tb.Th in mm), trabecular number (Tb.N in mm^{-1}), and trabecular separation (Tb.Sp in mm) from

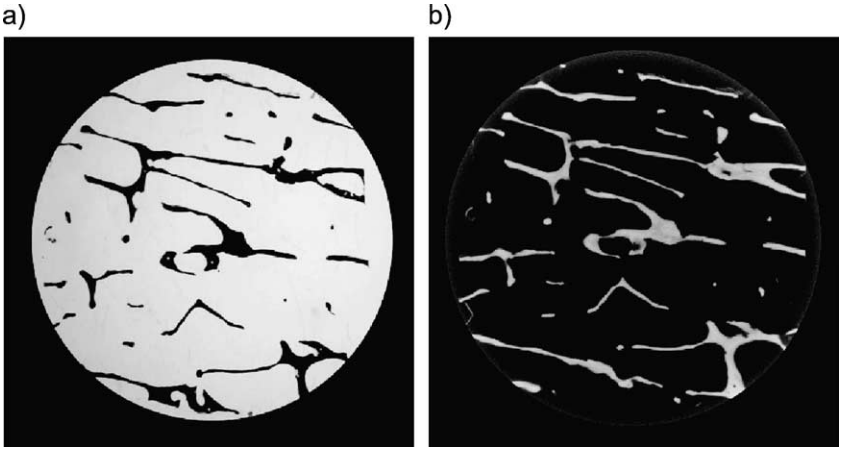

Fig. 2. Comparison between (a) a histological slice cut from the sample and (b) the corresponding slice extracted from a 3D SR μCT image (voxel size = 10 μm).

BV/TV and bone surface (BS). In addition, direct parameters were also evaluated. The direct trabecular thickness (Tb.Th*) was computed using the model-independent method described by Hildebrand [27]. The Euler-Poincaré Number was computed from the 3D digital images according to the method described by Odgaard and Gundersen [28]. After normalization to the bone volume, the Euler density (in mm^{-3}) was obtained. For a connected bone trabecular structure without closed cavities, the Euler Number characterizes 3D connectivity: as connectivity increases, the Euler density decreases. The 3D-fractal dimension was computed according to the generalization of the box counting method described in 2D by Weinstein et al. [17,30]. The fractal dimension is defined as the slope of the linear part of the curve $\log(N(\varepsilon))$ versus $\log(\varepsilon)$, where $N(\varepsilon)$ is the number of boxes including bone interface and ε is the box edge size. Applying this method to 3D digital images yields a 3D-fractal dimension ranging between 2 and 3. In our study, the 3D fractal dimension was computed from 40 μm spatial resolution images. Architectural anisotropy was also measured. The MIL distribution was interpolated by an ellipsoid giving the three main architectural directions and the associated MIL values: $MIL_1 > MIL_2 > MIL_3$. Taking into account the method of sample cutting, the directions 1, 2, and 3 were, respectively, close to the main directions of the superior trabecular network (Z axis), of the inferior trabecular network (X axis), and of the medio-lateral direction (Y axis).

2D morphometric analysis

One of the lateral samples was embedded in methylmethacrylate, imaged using 3D μCT as previously described and a 7-μm-thick histological section was cut. Fig. 2 displays the resulting histological slice (b) and the corresponding slice extracted from the 3D μCT image (a) showing very good concordance between the two techniques. Thus, we used such tomographic slices for computing 2D morphometric parameters. For this purpose, three parallel slices 150-μm apart along the superior trabecular network (Z, Y plane) were extracted from the 3D images. Measurements were performed with an automatic image analyser using Morpho Expert® and Bone® software (Explora Nova®, France). In 2D, we used the parameter B.Ar/T.Ar representing the bone area compared to the tissue area. For strut analysis, we used a method derived from the technique described by Garrahan et al. [45], all the steps of skeletonization and detection of nodes, termini and associated struts were automatic with interactive correction if necessary. The following parameters were determined: total strut length (TSL) expressed by tissue volume (TV), number of nodes expressed by TV (N.Nd/TV), length of node to node expressed as a percentage of total strut length (Nd to Nd.Le/TSL), and the ratio of number of nodes by number of termini (N.Nd/N.Tm). The 2D fractal dimension was also computed using the box counting method [17].

Compressive tests

Unconstrained compressive testing was performed on an universal screw-driven machine (Schenck RSA 250). The compressive load was measured by a 5000 N load cell (TME®, F 501 TC) and the displacement was measured directly on the sample, using a specific displacement transducer developed at the LaMCoS (Laboratoire de Mécanique des Contacts et des Solides, INSA, Lyon, France) [20,46]. Samples equipped with the specific displacement transducer were placed in a saline solution at 37°C (Fig. 3).

All tests were performed at a displacement speed of 0.5 mm/min and preceded by 10 cycles of preloading. Preloading and non-destructive compression were limited to 0.6% of strain and performed successively in three orthogonal directions: the inferior network direction (X axis), the medio-lateral direction (Y axis), and the superior network direction (Z axis), determinated by radiographs. The Young's moduli E_X, E_Y, and E_Z were computed from the linear parts of the force-displacement curves and considering the apparent sections of the cubic sample. After that, a destructive test was carried out in the Z direction. The Young's modulus E and the maximum compressive stress σ_{max} were evaluated from the force-displacement curve, also considering the apparent section of the sample. E and E_Z, although measured during two different tests, give the same information.

Statistics

Descriptive statistics were summarized by mean value, standard deviation, median and range. Data or their logarithmic transformations ($\log E_Y$, $\log E_Z$, $\log E$, $\log E_X/E_Y$, $\log E_X/E_Y$) were normally distributed. Differences between 2D and 3D parameters were assessed by a paired

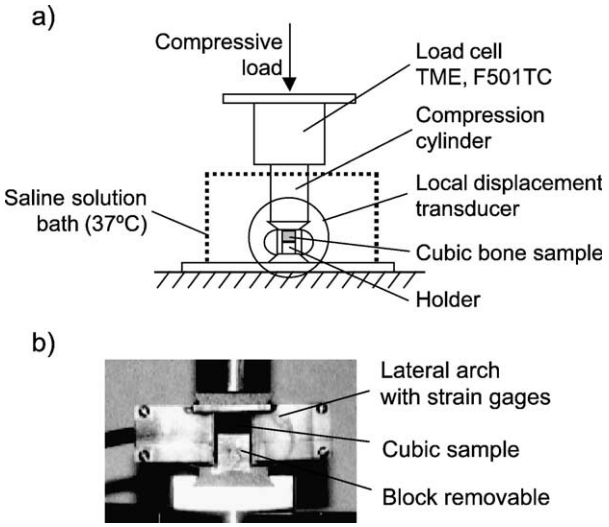

Fig. 3. Description of the equipment used for compressive tests. (a) Plan. (b) Local displacement transducer.

t test. Multiple correlations were performed using stepwise analysis for the selection of variables. The relationships between normally distributed parameters were evaluated by Pearson correlation coefficients. The degree of significance was assessed according to Bonferroni's procedure ($P \leq 0.01$ indicates a significant correlation). Unistat® software was used to perform statistical analysis.

Results

Compressive properties

Mechanical elastic properties in the three main directions X, Y, Z and the maximum compressive stress in the direction of the superior trabecular network are shown in Table 1. The elastic properties show a mechanical anisotropy corresponding to the anatomical anisotropy of the trabecular network in the posterior tuberosity of the calcaneus. The superior trabecular network shows the highest Young's modulus (E_Z) and the medio-lateral direction, the lowest (E_Y). In the direction of the superior trabecular network, the Young's modulus obtained during the elastic test (E_Z) and the value obtained from the destructive test (E) were significantly correlated ($r = 0.99$, $P < 0.0001$). The Young's modulus in the superior trabecular network (E) was also significantly correlated with the maximum compressive stress (σ_{max}) ($r = 0.90$, $P < 0.0001$).

3D and 2D morphometric measurement

A 3D digital image showing the main trabecular orientations and an extracted 2D slice are shown in Fig. 4.

Descriptive statistics concerning the morphological parameters obtained from 2D slices and from 3D digital images are summarized in Table 2. The 2D fractal dimensions ranged as expected between 1 and 2, with a mean (±SD) equal to 1.45 (±0.13). The 3D fractal dimensions ranged between 2 and 3, with a mean equal to 2.60 (±0.19). The mean Euler density was −4.42 (±1.80)/mm^3 and all values were negative. As also shown in Table 2, the 3D parameters were significantly correlated to the similar 2D parameters except Euler density vs. N.Nd/TV, Nd.N/Tm.N and Nd to Nd.Le/TSL. However, all differences between similar 2D and 3D parameters were significant except for BV/TV (Table 2). The two dimensional parameters (B.Ar/T.Ar, Tb.Th, Tb.N, Tb.Sp, N.Nd/TV, Nd.N/Tm.N, Nd.to.Nd.Le/TSL) were significantly correlated to each other ($0.49 < |r| < 0.96$, $0.0000 < P < 0.02$). Three-dimensional parameters (BV/TV, Tb.Th, Tb.Th*, Tb.N, Tb.Sp) were also significantly correlated to each other ($0.71 < |r| < 0.96$, $0.0000 < P < 0.0002$) except Euler density, which is only significantly correlated to Tb.N.

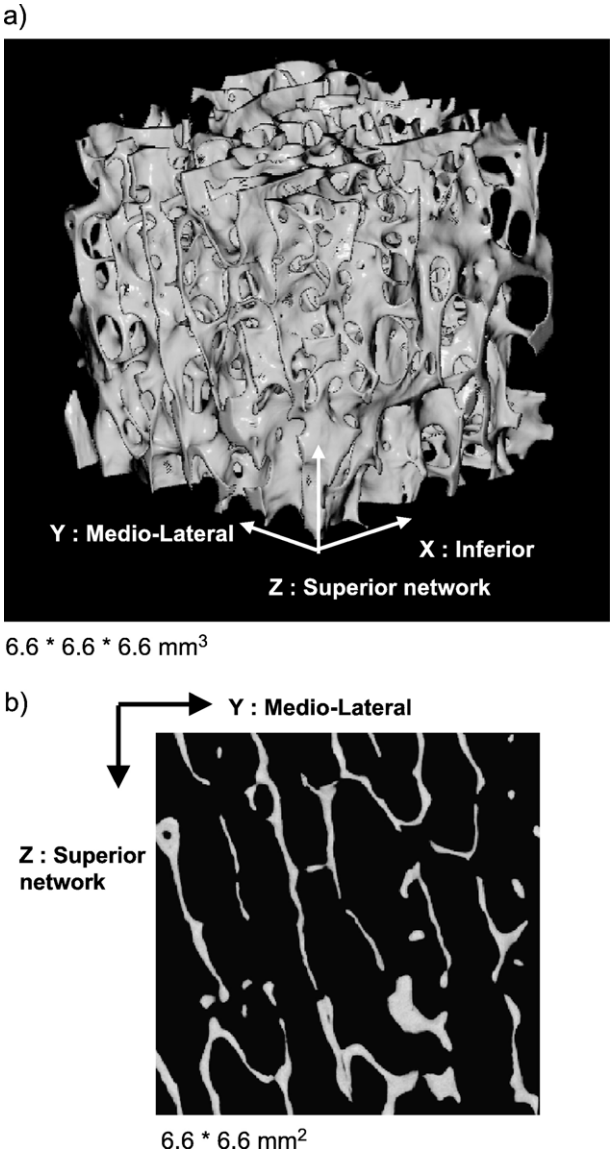

Fig. 4. Illustration of bone micro-architecture in one cubic sample (Male, 69 years, BV/TV = 12.8%) (a) 3D display of the 3D SR μCT image (voxel size = 10 μm) and (b) First histology-like slice.

Table 1
Mechanical properties of human calcanei (mean age 78 ± 9 years, $n = 16$, range [61–91 years])

Parameters	Cubic sample				
	n	Mean	SD	Median	Range
Biomechanics					
E_X (MPa)	16	84	72	67	3–258
E_Y (MPa)	16	57	70	27	2–225
E_Z (MPa)	16	318	330	221	11–1144
E_Z/E_X	16	3.6	1.8	3.5	0.65–8.0
E_Z/E_Y	16	7.5	7.3	5.1	1.38–32.0
E_X/E_Y	16	2.3	1.7	1.9	0.6–7.7
E (MPa)	16	297	303	218	6–1088
σ_{max} (MPa)	15	3.22	2.53	3.24	0.27–8.16

SD: standard deviation.
E_X, E_Y, E_Z: Young modulus along the X, Y, Z axis after non-destructive test. E: Young modulus along the Z axis after destructive test, σ_{max}: maximum compressive stress.

Table 2
2D and 3D morphological characteristics of human calcanei (mean age 79 ± 7 years, n = 17, range [61–91 years])

Morphometry (2D) from 3D					SR μCT 3D analysis					Comparison 2D vs. 3D	
n = 17	Mean	SD	Median	Range	n = 17	Mean	SD	Median	Range	Paired t test	Correlations
Structural parameters					*Architectural parameters*						
B.Ar/T.Ar (%)	11.3	4.6	10.6	3.14–18.97	BV/TV (%)	11.06	4.4	10.75	3.7–18.8	ns	r = 0.86, P < 0.0001
Tb.Th (μm)	114	25.6	118	61–165	Tb.Th (μm)	77	14.6	78	48–102	P < 0.0001	r = 0.83, P < 0.0001
					Tb.Th* (μm)	138	23	138	85–179	P < 0.0001	r = 0.87, P < 0.0001
Tb.Sp (μm)	1010	360	884	610–1881	Tb.Sp (μm)	717	248	654	423–1311	P < 0.0001	r = 0.87, P < 0.0001
Tb.N (/mm)	0.96	0.26	0.98	0.51–1.33	Tb.N (/mm)	1.36	0.36	1.34	0.74–1.92	P < 0.0001	r = 0.81, P < 0.0001
Irregularity					*Irregularity*						
Fractal dimension	1.45	0.13	1.46	1.2–1.61	Fractal dimension[a]	2.6	0.19	2.62	2.27–2.88	–	r = 0.87, P < 0.0001
Connectivity parameters					*Connectivity parameters*						
N.Nd/TV (/mm^2)	0.60	0.32	0.49	0.13–1.20	Euler density (/mm^3)	−4.42	1.80	−4.14	−8.32/−2.1	–	ns[b]
Nd to Nd.Le/TSL (%)	18.75	10.25	17.80	1.73–38						–	ns[c]
N.Nd/N.Tm	0.28	0.15	0.25	0.04–0.63						–	ns[d]
					Anisotropy						
					$MIL_{1(Z)}$	0.213	0.05	0.22	0.11–0.29		
					$MIL_{2(X)}$	0.15	0.03	0.15	0.10–0.20		
					$MIL_{3(Y)}$	0.13	0.0	0.14	0.08–0.18		
					$MIL_{1(Z)}/MIL_{2(X)}$	1.4	0.12	1.45	1.16–1.58		
					$MIL_{1(Z)}/MIL_{3(Y)}$	1.63	0.15	1.64	1.41–1.83		
					$MIL_{2(X)}/MIL_{3(Y)}$	1.17	0.12	1.12	1.01–1.54		

SD: standard deviation, B.Ar: bone area, T.Ar: tissue area, BV: bone volume, TV: tissue volume, Tb.Th: trabecular thickness, Tb.Th*: direct trabecular thickness, Tb.Sp: trabecular separation, Tb.N: trabecular number, N.Nd: Node number, Nd to Nd.Le/TSL: node to node length/total strut length, N.Nd/N.Tm: node number/terminus number, MIL: mean intercept length. Comparison between Euler density.

[a] Computed from 40 μm spatial resolution images.

[b] N.Nd/TV.

[c] Nd to Nd.Le/TSL.

[d] N.Nd/N.Tm.

Table 3
Pearson correlation coefficients (r) between the compressive properties and 2D and 3D morphological parameters

Morphometry						SR μCT 3D analysis (10 μm)					
$n = 16$	E_X	Log E_Y	Log E_Z	Log E	σ_{max} [†]	$n = 16$	E_X	Log E_Y	Log E_Z	Log E	σ_{max} [†]
Structural parameters						*Architectural parameters*					
B.Ar/T.Ar	0.87[a]	0.77[b]	0.76[b]	0.72[b]	0.84[a]	BV/TV	0.83[a]	0.91[a]	0.89[a]	0.87[a]	0.96[a]
Tb.Th	0.71[b]	0.71[b]	0.59[c]	0.56[c]	0.64[c]	Tb.Th	0.74[b]	0.91[a]	0.79[a]	0.78[b]	0.80[b]
						Tb.Th*	0.78[b]	0.86[a]	0.75[b]	0.74[b]	0.78[b]
Tb.Sp	−0.71[b]	−0.71[c]	−0.69[c]	−0.66[c]	−0.79[b]	Tb.Sp	−0.72[b]	−0.85[a]	−0.85[a]	−0.82[a]	−0.87[a]
Tb.N	0.74[b]	0.66[c]	0.71[b]	0.67[c]	0.84[a]	Tb.N	0.73[b]	0.80[b]	0.84[a]	0.82[a]	0.94[a]
Connectivity parameters						*Connectivity parameters*					
N.Nd/TV (/mm^2)	0.72[b]	0.53[d]	0.55[d]	0.48[d]	0.70[c]	Euler density	−0.13[e]	−0.05[e]	−0.27[e]	−0.23[e]	−0.36[e]
Nd to Nd.Le/TSL (%)	0.78[b]	0.56[d]	0.54[d]	0.48[d]	0.68[c]						
N.Nd/N.Tm	0.77[b]	0.57[c]	0.59[c]	0.54[d]	0.70[c]						
Irregularity						*Irregularity*					
Fractal dimension[†]	0.78[b]	0.75[b]	0.71[b]	0.68[c]	0.86[a]	Fractal dimension[‡]	0.71[b]	0.81[b]	0.87[a]	0.85[a]	0.93[a]

E_X, E_Y, E_Z: Young modulus along the X, Y, Z axis after non-destructive test, E: Young modulus along the Z axis after destructive test, σ_{max}: maximum compressive stress. B.Ar: bone area, T.Ar: tissue area, BV: bone volume, TV: tissue volume, Tb.Th: trabecular thickness, TbTh*: direct trabecular thickness, Tb.Sp: trabecular separation Tb.N: trabecular number, N.Nd: Node number, Nd to Nd.Le/TSL: node to node length/total strut length, N.Nd/N.Tm: node number/terminus number, MIL: mean intercept length.

[a] $P < 0.0001$.

[b] $P < 0.001$.

[c] $P < 0.01$, 0.01<.

[d] $P < 0.05$.

[e] not significant.

[†] $n = 15$.

[‡] Computed from 40 μm spatial resolution images.

Relationship between compressive properties and morphometric measurements

The Pearson correlation coefficients between mechanical parameters and morphological parameters assessed in 2D and 3D are given in the Table 3. E and σ_{max} were significantly correlated to all 2D and 3D parameters excepted for Euler density (Figs. 5a, b, c).

In 2D, 52% of the variance of the Young's modulus (E) and 71% of the variance of the maximum compressive stress

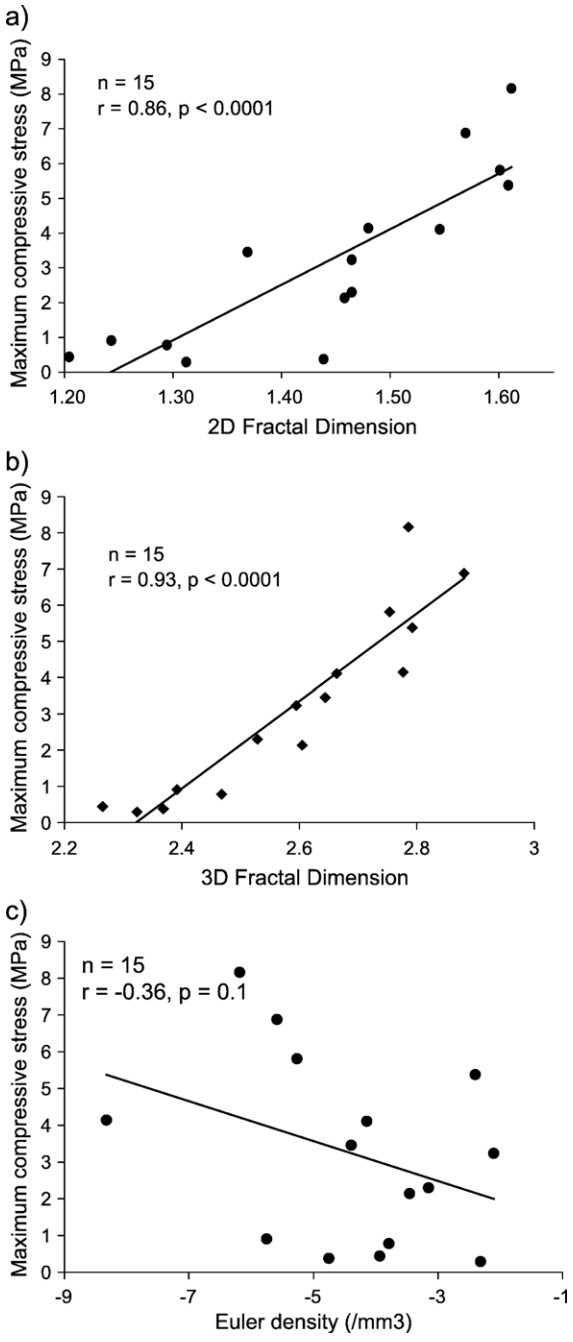

Fig. 5. Correlations between maximum compressive strength and (a) 2D fractal dimension, (b) 3 D fractal dimension and (c) Euler density.

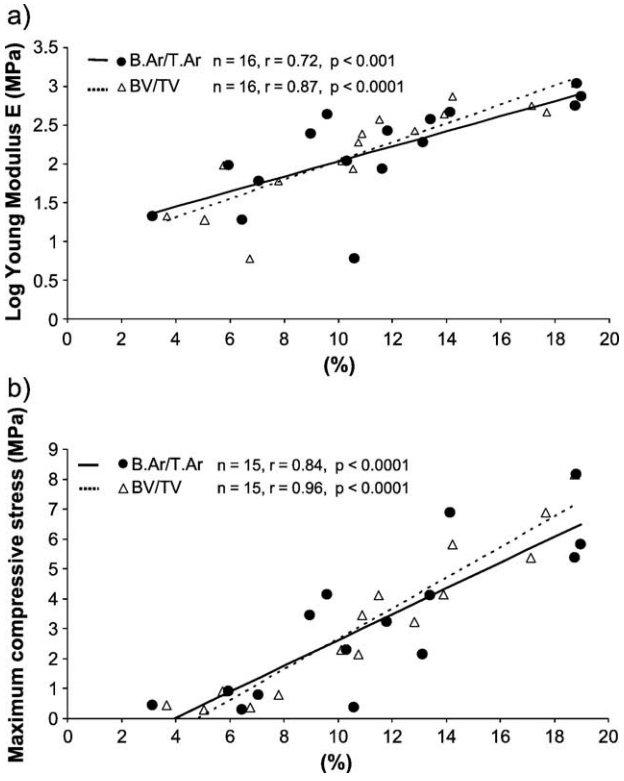

Fig. 6. Correlations between (a) Young's modulus and B.Ar/T.Ar-BV/TV and (b) maximum compressive stress and B.Ar/T.Ar-BV/TV.

(σ_{max}) were explained by the B.Ar/T.Ar (Fig. 6a). The main 2D determinants of the maximum compressive stress (σ_{max}) were either the B.Ar/T.Ar or the 2D fractal dimension. However, these two 2D parameters are highly correlated. After adjustment for B.Ar/T.Ar, correlations between mechanical properties and 2D morphological parameters were no longer significant. Concerning the Young's modulus (E), the B.Ar/T.Ar was the main explanatory variable.

In 3D, 76% of the variance of the Young's modulus (E) and 92% of the variance of the maximum compressive stress (σ_{max}) were explained by the BV/TV (Fig. 6b). As shown in Table 4, correlations between the Young moduli E_X, E_Y, and E_Z and the corresponding MIL were significant. No significant correlation was found between the MIL ratio and the mechanical anisotropy. In 3D, σ_{max} was mainly explained by BV/TV and Tb.Th ($\sigma_{max} = f$(BV/TV): $r = 0.96$, $P < 0.0001$; σ_{max} = f(BV/TV, Tb.Th): $r = 0.98$, $P < 0.0001$). After adjusting for BV/TV, only the correlation between σ_{max} and trabecular thickness remained significant ($r = -0.65$, $P < 0.006$ for Tb.Th). However, it should be noticed that BV/TV and Tb.Th were highly correlated together and that its introduction in the regression analysis was questionable.

Discussion

This study has demonstrated that when considering 3D parameters, mechanical properties of human cancellous os

Table 4
Pearson correlation coefficients (r) between the mechanical and architectural anisotropy parameters

$n = 16$	SR μCT 3D analysis (10 μm)						
	E_Z	E_X	E_Y	E_Z/E_X	E_Z/E_Y	E_X/E_Y	σ_{max}*
$MIL_{1(Z)}$	0.80[a]						0.78[b]
$MIL_{2(X)}$		0.77[c]					0.83[b]
$MIL_{3(Y)}$			0.90[a]				0.79[b]
$MIL_{1(Z)}/MIL_{2(X)}$				−0.0[d]			0.18[d]
$MIL_{1(Z)}/MIL_{3(Y)}$					−0.22[d]		0.45[d]
$MIL_{2(X)}/MIL_{3(Y)}$						−0.15[d]	0.37[d]

E_X, E_Y, E_Z: Young modulus along the X, Y, Z axis after non-destructive test.
σ_{max}: maximum compressive stress, MIL: mean intercept length.
[a] $P < 0.0001$.
[b] $P < 0.01$.
[c] $P < 0.001$.
[d] not significant.
* $n = 15$.

calcis were explained only by BV/TV. According to Keaveny and Yeh [47], the available evidence suggests there is only a subtle sex effect on age-related changes in mean trabecular thickness, and for vertebral bone, Tb.Th is highly and linearly correlated with bone volume fraction. In our study, Tb.Th also improved significantly the prediction of compressive strength although it is highly correlated with BV/TV. TbTh could represent quality in material, which may contribute to strength of bone. Thereby, the parameter Tb.Th could not be added in a multiple regression analysis due to the highly correlation between it and BV/TV. The prediction of mechanical properties was not significantly improved by adding other 3D microarchitecture parameters (Tb.Th*, Tb.N, Tb.Sp), connectivity, and anisotropy. When limited to 2D dimensions, B.Ar/T.Ar and 2D Fractal dimension explain the mechanical properties, even if these parameters are highly correlated.

The compression protocol used in this study and previously published [20], allowed the mechanical characterization of the cancellous bone in environmental conditions (saline solution at 37°C), close to the in vivo conditions. However, since cubic samples had a limited size and were not confined, the real in vivo conditions were not exactly reproduced. The experimental protocol could introduce end artifacts that inherently lead to an under prediction of the in vivo trabecular stiffness [48]. Previously, Goulet et al. [49] had studied the relationship between the structural and orthogonal compressive properties of trabecular bone. This emphasizes the great variability of the mechanical properties of cancellous bone related to both microarchitecture and direction of the main trabecular network relatively to the loading direction. But, significant correlations have been obtained between the Young's modulus and the compressive strength in the direction of the superior trabecular network: results obtained by Mitton et al. [50] in the same direction and Langton et al. [51] in the medio-lateral direction. The mechanical anisotropy, expressed by $E_Z > E_X > E_Y$, corresponds to the trabecular network anisotropy of this anatomical site [52]. The superior network (Z), which is greatly loaded in vivo is the stiffest direction and the medio-lateral direction (Y) which is not loaded in vivo is the weakest.

The 2D morphometry is usually considered as the standard method to quantify cancellous bone architecture. In 2D, Chappard et al. [53] compared eight histomorphometric methods known to characterize the architecture of trabecular bone (154 male osteoporotic patients, transiliac bone biopsies). They studied relationships between the various architectural parameters. In particular, they found a linear correlation between bone volume and several histomorphometric parameters (Tb.Th, Tb.N). This was easily explained by the calculation of Tb Th and TbN, which were derived from Bone area and perimeter [1].

Instead of histological embedded slices, we used slices extracted from the 3D μCT images, after showing that they provided the same information. The agreement between the two techniques has already been reported in several other works [20,54–57]. Our methodology allowed all measurements (2D and 3D micro-architecture, mechanical tests) on the same sample. The 2D analysis technique employed was that typical used in histomorphometry. However, it uses a plate model assumption, which is not true for all bones. The architectural parameters computed from the 3D images are in good agreement with the values reported in Hildebrand et al. [32] on the same site using 3D X-ray μCT at a spatial resolution of 28 μm, with mean BV/TV of 12% instead of 11.1% found in our study, and mean number of trabeculae of 1.027/mm (Tb.N* = 1.46/mm) and of 1.36/mm, respectively. It is interesting to note that the trabecular thickness (Tb.Th) appears underestimated in both studies when computed from the 3D MIL method (95 μm and 77 μm in our study), but that the mean direct trabecular thickness (Tb.Th*) and the mean value of the trabecular thickness evaluated these authors are very comparable (138 and 129 μm, respectively). Our values for 3D fractal dimensions (2.6 ± 0.19) are higher than those

recently published by Uchiyama et al. [58] (2.21 ± 0.05) for vertebrae cancellous bone, showing a less irregular network in the calcaneus than in the vertebra. Our values of Euler density are close to those already published for different human sites [59,60].

The mechanical properties of the cancellous bone are significantly correlated with most of the morphological parameters. These results are akin to those in the literature for different human sites, using different architectural analyses and different mechanical characterization methods [5,18,20,31,60]. Yet, the Pearson coefficients obtained for the correlations between the mechanical properties and the 2D or 3D structural parameters are close. The nonsignificant correlations between the MIL ratios and mechanical anisotropy (Table 4) can be explained by the tested directions which were slightly different from the natural directions (located by *X*-rays).

Our study demonstrated that the integration of the 2D micro-architectural parameters did not improve the correlation between the compressive strength and the 2D bone volume fraction. It could mean that the direction of trabecular network and its connectivity estimated from 2D slices do not bring additional information to the estimation of the compressive strength. The introduction of 3D architectural parameters, in addition to the BV/TV, did not significantly improve the prediction of the compressive strength. This is also valid for Tb.Th due to the fact that BV/TV and Tb.Th were highly correlated together. Even if significant correlations between architectural and mechanical properties are published in the literature, the fact that 3D standard parameters, 3D connectivity or 3D fractal dimension, can improve the assessment of the compressive strength by the bone volume fraction has not been well demonstrated. Kabel et al. [60] concluded that the integration of the connectivity density in the multiple correlation, marginally improves the correlation between the mechanical stiffness and the bone volume fraction, whereas Ulrich et al. [61] concluded there was a real improvement. In other respects, the fabric tensor built from MIL parameters has largely been used with the bone volume fraction to estimate the elastic properties of cancellous bone [34,62].

We acknowledge that this study presents some limitations. There is little variability in the type of structures because of the narrow range of ages and without any pathology which could lead to particular structure called ‘critical’ by Ulrich et al. [61]. This can explain the difficulties encountered in determining the contribution of each characteristics of the trabecular network-volume fraction, orientation, connectivity, in the mechanical strength. However, the range of our data was wide. Moreover, only bone volume and architectural parameters are considered to explain the mechanical properties. The intrinsic properties of bone tissue such as the mean degree of mineralization were not taken into account, but are actually being studied by another research team [63].

To our knowledge, our study is the first permitting the comparison of relationships between 2D or 3D morphological parameters and mechanical properties. Significant correlations were found between morphological parameters evaluated in 2D or 3D, and the mechanical properties of the os calcis. The addition of 2D parameters, reflecting connectivity and anisotropy of the network to B.Ar/T.Ar did not improve the estimation of compressive strength. In 3D, even if the introduction of the Tb.Th with the BV/TV brought a significant improvement in the prediction of the compressive strength, this conclusion may be moderated by the fact that the two parameters were found highly correlated.

References

[1] Parfitt AM, Mathews CH, Villanueva AR, Kleerekoper M, Frame B, Rao DS. Relationships between surface, volume, and thickness of iliac trabecular bone in aging and in osteoporosis. Implications for the microanatomic and cellular mechanisms of bone loss. J Clin Invest 1983;72:1396–409.
[2] Aaron JE, Makins NB, Sagreiya K. The microanatomy of trabecular bone loss in normal aging men and women. Clin Orthop 1987: 260–71.
[3] Mellish RW, Garrahan NJ, Compston JE. Age-related changes in trabecular width and spacing in human iliac crest biopsies. Bone Miner 1989;6:331–8.
[4] Recker RR. Low bone mass may not be the only cause of skeletal fragility in osteoporosis. Proc Soc Exp Biol Med 1989;191:272–4.
[5] Fyhrie DP, Schaffler MB. Failure mechanisms in human vertebral cancellous bone. Bone 1994;15:105–9.
[6] Majumdar S, Link TM, Augat P, Lin JC, Newitt D, Lane NE, et al. Trabecular bone architecture in the distal radius using magnetic resonance imaging in subjects with fractures of the proximal femur. Magnetic Resonance Science Center and Osteoporosis and Arthritis Research Group. Osteoporos Int 1999;10:231–9.
[7] Goldstein SA. The mechanical properties of trabecular bone: dependence on anatomic location and function. J Biomech 1987;20:1055–61.
[8] Hodgskinson R, Currey JD. The effect of variation in structure on the Young’s modulus of cancellous bone: a comparison of human and non-human material. Proc Inst Mech Eng [H] 1990;204:115–21.
[9] Kleerekoper M, Villanueva AR, Stanciu J, Rao DS, Parfitt AM. The role of three-dimensional trabecular microstructure in the pathogenesis of vertebral compression fractures. Calcif Tissue Int 1985;37:594–7.
[10] Whitehouse WJ. The quantitative morphology of anisotropic trabecular bone. J Microsc 1974;101(Pt. 2):153–68.
[11] Ruegsegger P, Koller B, Muller R. A microtomographic system for the nondestructive evaluation of bone architecture. Calcif Tissue Int 1996;58:24–9.
[12] Link TM, Majumdar S, Lin JC, Newitt D, Augat P, Ouyang X, et al. A comparative study of trabecular bone properties in the spine and femur using high resolution MRI and CT. J Bone Miner Res 1998;13:122–32.
[13] Parfitt AM, Drezner MK, Glorieux FH, Kanis JA, Malluche H, Meunier PJ, et al. Bone histomorphometry: standardization of nomenclature, symbols, and units. Report of the ASBMR Histomorphometry Nomenclature Committee. J Bone Miner Res 1987; 2:595–610.
[14] Levitz P, Tchoubard D. Disorder porous solids: from chord distribution to small angle scattering. J Phys I France 1992;2:771–90.
[15] Mellish RW, Ferguson-Pell MW, Cochran GV, Lindsay R, Dempster DW. A new manual method for assessing two-dimensional

cancellous bone structure: comparison between iliac crest and lumbar vertebra. J Bone Miner Res 1991;6:689–96.
[16] Hahn M, Vogel M, Pompesius-Kempa M, Delling G. Trabecular bone pattern factor—A new parameter for simple quantification of bone microarchitecture. Bone 1992;13:327–30.
[17] Weinstein RS, Majumdar S. Fractal geometry and vertebral compression fractures. J Bone Miner Res 1994;9:1797–802.
[18] Fazzalari NL, Parkinson IH. Fractal dimension and architecture of trabecular bone. J Pathol 1996;178:100–5.
[19] Majumdar S, Newitt D, Mathur A, Osman D, Gies A, Chiu E, et al. Magnetic resonance imaging of trabecular bone structure in the distal radius: relationship with X-ray tomographic microscopy and biomechanics. Osteoporos Int 1996;6:376–85.
[20] Cendre E, Mitton D, Roux JP, Arlot ME, Duboeuf F, Burt-Pichat B, et al. High-resolution computed tomography for architectural characterization of human lumbar cancellous bone: relationships with histomorphometry and biomechanics. Osteoporos Int 1999; 10:353–60.
[21] Zysset PK, Sonny M, Hayes WC. Morphology–mechanical property relations in trabecular bone of the osteoarthritic proximal tibia. J Arthroplasty 1994;9:203–16.
[22] Goldstein SA, Goulet R, McCubbrey D. Measurement and significance of three-dimensional architecture to the mechanical integrity of trabecular bone. Calcif Tissue Int 1993;53(Suppl. 1): S127–32 [discussion S32-3].
[23] Muller R, Hahn M, Vogel M, Delling G, Ruegsegger P. Morphometric analysis of noninvasively assessed bone biopsies: comparison of high-resolution computed tomography and histologic sections. Bone 1996;18:215–20.
[24] Feldkamp LA, Goldstein SA, Parfitt AM, Jesion G, Kleerekoper M. The direct examination of three-dimensional bone architecture in vitro by computed tomography. J Bone Miner Res 1989;4:3–11.
[25] Nuzzo S, Lafage-Proust MH, Martin-Badosa E, Boivin G, Thomas C, Alexandre C, et al. Synchrotron radiation microtomography allows the analysis of three-dimensional microarchitecture and degree of mineralization of human iliac crest biopsy specimens: effects of etidronate treatment. J Bone Miner Res 2002;17: 1372–82.
[26] Muller R, Hildebrand T, Ruegsegger P. Non-invasive bone biopsy: a new method to analyse and display the three-dimensional structure of trabecular bone. Phys Med Biol 1994;39:145–64.
[27] Hildebrand T, Ruegsegger P. A new method for the model-independent assessment of thickness in three-dimensional images. J Microsc 1997;185:67–75.
[28] Odgaard A, Gundersen HJ. Quantification of connectivity in cancellous bone, with special emphasis on 3-D reconstructions. Bone 1993;14:173–82.
[29] Harrigan TP, Mann RW. Characterisation of microstructural anisotropy in orthotropic materials using a second rank tensor. J Mater Sci 1984;19:761–7.
[30] Mawatari T, Miura H, Higaki H, Kurata K, Murakami T, Iwamoto Y. Quantitative analysis of three dimensional complexity and connectivity changes in trabecular architecture in relation with ageing and menopause. Med Biol Eng Comput 1997;35:204.
[31] Majumdar S, Kothari M, Augat P, Newitt DC, Link TM, Lin JC, et al. High-resolution magnetic resonance imaging: three-dimensional trabecular bone architecture and biomechanical properties. Bone 1998;22:445–54.
[32] Hildebrand T, Laib A, Muller R, Dequeker J, Ruegsegger P. Direct three-dimensional morphometric analysis of human cancellous bone: microstructural data from spine, femur, iliac crest, and calcaneus. J Bone Miner Res 1999;14:1167–74.
[33] Borah B, Dufresne TE, Cockman MD, Gross GJ, Sod EW, Myers WR, et al. Evaluation of changes in trabecular bone architecture and mechanical properties of minipig vertebrae by three-dimensional magnetic resonance microimaging and finite element modeling. J Bone Miner Res 2000;15:1786–97.
[34] Zysset PK, Ominsky MS, Goldstein SA. A novel 3D micro-structural model for trabecular bone: I. The relationship between fabric and elasticity. Comput Methods Biomech Biomed Engin 1998;1:321–31.
[35] Muller R, Koller B, Hildebrand T, Laib A, Gianolini S, Ruegsegger P. Resolution dependency of microstructural properties of cancellous bone based on three-dimensional mu-tomography. Technol Health Care 1996;4:113–9.
[36] Peyrin F, Salome M, Cloetens P, Laval-Jeantet AM, Ritman E, Ruegsegger P. Micro-CT examinations of trabecular bone samples at different resolutions: 14, 7 and 2 micron level. Technol Health Care 1998;6:391–401.
[37] Kinney JH, Ladd AJC, Haupt DL, Majumdar S. Direct incorporation of 3-dimensional micro-tomography data into an elastic model of human trabecular bone. Bone 1996;19:146S.
[38] Salome M, Peyrin F, Cloetens P, Odet C, Laval-Jeantet AM, Baruchel J, et al. A synchrotron radiation microtomography system for the analysis of trabecular bone samples. Med Phys 1999;26: 2194–204.
[39] Vogel JM, Wasnich RD, Ross PD. The clinical relevance of calcaneus bone mineral measurements: a review. Bone Miner 1988;5:35–58.
[40] Wasnich RD, Ross PD, Heilbrun LK, Vogel JM. Selection of the optimal skeletal site for fracture risk prediction. Clin Orthop 1987:262–9.
[41] Pal GP, Routal RV. Architecture of the cancellous bone of the human talus. Anat Rec 1998;252:185–93.
[42] Ashman RB, Cowin SC, Van Buskirk WC, Rice JC. A continuous wave technique for the measurement of the elastic properties of cortical bone. J Biomech 1984;17:349–61.
[43] Peyrin F, Salome M, Nuzzo S, Cloetens P, Laval-Jeantet AM, Baruchel J. Perspectives in three-dimensional analysis of bone samples using synchrotron radiation microtomography. Cell Mol Biol (Noisy-le-grand) 2000;46:1089–102.
[44] Simmons CA, Hipp JA. Method-based differences in the automated analysis of the three-dimensional morphology of trabecular bone. J Bone Miner Res 1997;12:942–7.
[45] Garrahan NJ, Mellish RW, Compston JE. A new method for the two-dimensional analysis of bone structure in human iliac crest biopsies. J Microsc 1986;142(Pt. 3):341–9.
[46] Mitton D, Cendre E, Roux JP, Arlot ME, Peix G, Rumelhart C, et al. Mechanical properties of ewe vertebral cancellous bone compared with histomorphometry and high-resolution computed tomography parameters. Bone 1998;22:651–8.
[47] Keaveny TM, Yeh OC. Architecture and trabecular bone—Toward an improved understanding of the biomechanical effects of age, sex and osteoporosis. J Musculoskelet Neuron Interact 2002;2:205–8.
[48] Keaveny TM, Pinilla TP, Crawford RP, Kopperdahl DL, Lou A. Systematic and random errors in compression testing of trabecular bone. J Orthop Res 1997;15:101–10.
[49] Goulet RW, Goldstein SA, Ciarelli MJ, Kuhn JL, Brown MB, Feldkamp LA. The relationship between the structural and orthogonal compressive properties of trabecular bone. J Biomech 1994;27:375–89.
[50] Mitton D, Rumelhart C, Hans D, Meunier PJ. The effects of density and test conditions on measured compression and shear strength of cancellous bone from the lumbar vertebrae of ewes. Med Eng Phys 1997;19:464–74.
[51] Langton CM, Njeh CF, Hodgskinson R, Currey JD. Prediction of mechanical properties of the human calcaneus by broadband ultrasonic attenuation. Bone 1996;18:495–503.
[52] Jensen NC, Madsen LP, Linde F. Topographical distribution of trabecular bone strength in the human os calcanei. J Biomech 1991;24:49–55.
[53] Chappard D, Legrand E, Audran M, Basle MF. Histomorphometric measurement of the architecture of the trabecular bone in osteoporosis: comparative study of several methods. Morphologie 1999; 83:17–20.

[54] Fajardo RJ, Muller R. Three-dimensional analysis of nonhuman primate trabecular architecture using micro-computed tomography. Am J Phys Anthropol 2001;115:327–36.
[55] Fajardo RJ, Ryan TM, Kappelman J. Assessing the accuracy of high-resolution X-ray computed tomography of primate trabecular bone by comparisons with histological sections. Am J Phys Anthropol 2002;118:1–10.
[56] Engelke K, Graeff W, Meiss L, Hahn M, Delling G. High spatial resolution imaging of bone mineral using computed microtomography. Comparison with microradiography and undecalcified histologic sections. Invest Radiol 1993;28:341–9.
[57] Kuhn JL, Goldstein SA, Feldkamp LA, Goulet RW, Jesion G. Evaluation of a microcomputed tomography system to study trabecular bone structure. J Orthop Res 1990;8:833–42.
[58] Uchiyama T, Tanizawa T, Muramatsu H, Endo N, Takahashi HE, Hara T. Three-dimensional microstructural analysis of human trabecular bone in relation to its mechanical properties. Bone 1999;25:487–91.
[59] Ding M, Odgaard A, Hvid I. Accuracy of cancellous bone volume fraction measured by micro-CT scanning. J Biomech 1999;32:323–6.
[60] Kabel J, Odgaard A, van Rietbergen B, Huiskes R. Connectivity and the elastic properties of cancellous bone. Bone 1999;24:115–20.
[61] Ulrich D, van Rietbergen B, Laib A, Ruegsegger P. The ability of three-dimensional structural indices to reflect mechanical aspects of trabecular bone. Bone 1999;25:55–60.
[62] Kabel J, Van Rietbergen B, Odgaard A, Ruiskes R. Fabric and volume fraction can accurately predict mechanical properties for a wide range of trabecular architectures. In Transaction of the 43rd Annual Meeting, Orthop. Res. Soc. 1997. p. 800 [San Fransisco, CA] ISSN 0149-6433.
[63] Follet H, Boivin G, Rumelhart C, Meunier PJ. The degree of mineralization is a determinant of bone strength: a study on human calcanei. Bone 2004;34:783–9.
[64] Kapandji IA. Physiologie articulaire: schémas commentés de mécanique humaine. fifth ed. Tronc et rachis: le rachis dans son ensemble, la ceinture pelvienne et les articulations sacro-iliaques, le rachis lombaire, le rachis dorsal et la respiration, le rachis cervicalx, vol. 3. Paris: Maloine; 1994. p. 255.
[65] Putz R, Pabst R, Sobotta J. Atlas d'Anatomie humaine, vol. 1. Paris: Editions medicales Internationales, 1994. 416 pp.